

GAIA PROPER MOTIONS AND ORBITS OF THE ULTRA-FAINT MILKY WAY SATELLITES

JOSHUA D. SIMON

Observatories of the Carnegie Institution for Science, 813 Santa Barbara St., Pasadena, CA 91101
Draft version June 8, 2018

ABSTRACT

The second data release from the *Gaia* mission (DR2) provides a comprehensive and unprecedented picture of the motions of astronomical sources in the plane of the sky, extending from the solar neighborhood to the outer reaches of the Milky Way. I present proper motion measurements based on *Gaia* DR2 for 17 ultra-faint dwarf galaxies within 100 kpc of the Milky Way. I compile the spectroscopically-confirmed member stars in each dwarf bright enough for *Gaia* astrometry from the literature, producing member samples ranging from 2 stars in Triangulum II to 68 stars in Boötes I. From the spectroscopic member catalogs I estimate the proper motion of each system. I find good agreement with the proper motions derived by the *Gaia* collaboration for Boötes I and Leo I. The tangential velocities for 14 of the 17 dwarfs are determined to better than 50 km s^{-1} , more than doubling the sample of such measurements for Milky Way satellite galaxies. The orbital pericenters are well-constrained, with a median value of 38 kpc. Only one satellite, Tucana III, is on an orbit passing within 15 kpc of the Galactic center, suggesting that the remaining ultra-faint dwarfs are unlikely to have experienced severe tidal stripping. As a group, the ultra-faint dwarfs are on high-velocity, eccentric, retrograde trajectories, with nearly all of them having space motions exceeding 370 km s^{-1} . A large majority of the objects are currently close to the pericenters of their orbits. In a low-mass ($M_{\text{vir}} = 0.8 \times 10^{12} M_{\odot}$) Milky Way potential, eight out of the 17 galaxies lack well-defined apocenters and appear likely to be on their first infall, indicating that the Milky Way mass may be larger than previously estimated or that many of the ultra-faint dwarfs are associated with the Magellanic Clouds. The median eccentricity of the ultra-faint dwarf orbits is 0.79, similar to the values seen in numerical simulations, but distinct from the rounder orbits of the more luminous dwarf spheroidals.

Subject headings: astrometry; dark matter; galaxies: dwarf; galaxies: kinematics and dynamics; Local Group

1. INTRODUCTION

The orbits of dwarf galaxies around the Milky Way can provide crucial information regarding the mass and mass profile of the Galaxy (e.g., Boylan-Kolchin et al. 2013), the formation and evolution of dwarf galaxies (e.g., Peñarrubia et al. 2008), the history of the Local Group (e.g., Rocha et al. 2012), and perhaps even the properties of dark matter (e.g., McGaugh & Wolf 2010). A particularly striking example is the Magellanic Clouds and the origin of the Magellanic Stream: the large tangential velocity of the Clouds measured by Kallivayalil et al. (2006, 2013) suggests that the LMC and SMC have completed at most one passage around the Milky Way (Besla et al. 2007), which significantly changes models for the formation of the stream (Nidever et al. 2008; Besla et al. 2010; Diaz & Bekki 2011, 2012; D’Onghia & Fox 2016).

Until now, proper motions of Milky Way satellite galaxies have been determined painstakingly, either with multiple epochs of *Hubble Space Telescope* imaging (e.g., Piatek et al. 2002, 2003; Lépine et al. 2011; Sohn et al. 2013; Pryor et al. 2015) or with longer time baselines from ground-based data (e.g., Dinescu et al. 2005; Méndez et al. 2010; Casetti-Dinescu & Girard 2016; Casetti-Dinescu et al. 2018). These measurements have been limited to the Magellanic Clouds and the relatively luminous ($L \gtrsim 2 \times 10^5 L_{\odot}$) classical dwarf

spheroidal (dSph) galaxies and have typical uncertainties of $\sim 0.1 \text{ mas yr}^{-1}$. In some cases, measurements by different groups and with different techniques disagree by more than the quoted uncertainties, suggesting the possibility of systematic errors (Piatek et al. 2007; Méndez et al. 2010; Pryor et al. 2015; Casetti-Dinescu & Girard 2016). The only existing proper motions for ultra-faint ($L \lesssim 10^5 L_{\odot}$) dwarf galaxies are the recent determination for Segue 1 by Fritz et al. (2017) and the *Gaia* team’s just-released measurement of Boötes I (Gaia Collaboration et al. 2018b).

With the second data release (DR2; Gaia Collaboration et al. 2018a) from the *Gaia* mission (Gaia Collaboration et al. 2016), proper motion measurements for Milky Way satellites will become routine. For objects nearby enough to have appreciable motions in the plane of the sky, identification of bright member stars in a satellite will be sufficient to determine its tangential velocity with accuracy similar to the best presently existing measurements. The relationship between proper motion and transverse velocity is

$$v_{\text{tan}} = 474 \left(\frac{\mu}{1 \text{ mas yr}^{-1}} \right) \left(\frac{d}{100 \text{ kpc}} \right) \text{ km s}^{-1}, \quad (1)$$

where μ is the proper motion in mas yr^{-1} and d is the distance in kpc. Thus, a proper motion accuracy of 0.1 mas yr^{-1} corresponds to a velocity accuracy bet-

ter than 50 km s^{-1} at 100 kpc, comparable to the *HST* proper motions of the classical dSphs. In the *Gaia* DR2 catalog, the proper motion for a single star at magnitude ~ 16 , such as a giant near the tip of the red giant branch at ~ 60 kpc, is measured at this level. For a dwarf galaxy containing multiple stars at magnitude ~ 18 , more accurate measurements can be obtained by averaging the *Gaia* proper motions for all of the known member stars.

To date, proper motion measurements, and hence three-dimensional velocity vectors, have only been published for 13 Milky Way satellites. A substantially larger set of space motions in the outer halo of the Milky Way can now be determined. In concert with new constraints from stellar streams (Bonaca & Hogg 2018), these measurements will provide a significant new sample of tracers of the Milky Way’s gravitational potential for inferring the mass of the Galaxy (e.g., Battaglia et al. 2005; Sales et al. 2007; Lux et al. 2010; Watkins et al. 2010; Boylan-Kolchin et al. 2013; Barber et al. 2014; Patel et al. 2018).

In this paper I present the first proper motion measurements for a large sample of nearby ultra-faint dwarf galaxies. In Section 2 I compile confirmed member stars in each galaxy that are bright enough for accurate *Gaia* astrometry. In Section 3 I test for possible systematics in the *Gaia* proper motions of distant and faint stars using systems with well-measured proper motions. In Section 4 I use the member catalogs for each dwarf to determine their proper motions. I then compute the corresponding orbits around the Milky Way in Section 5. I discuss the implications of the orbits in Section 6 and conclude in Section 7.

2. MEMBER SAMPLES

Motivated by the lack of available proper motions for ultra-faint dwarf galaxies and the velocity accuracy discussed above, for this study I select a sample of dwarf galaxies with $M_V > -8$ and $d < 100$ kpc. Although there are 25 confirmed or likely dwarfs meeting these criteria, not all of those objects have published spectroscopy, meaning that member stars cannot be confidently separated from non-members. Therefore, for the remainder of this paper I limit consideration to the 17 ultra-faint dwarfs for which spectroscopic member catalogs are available. When possible, I supplement the spectroscopic samples with RR Lyrae stars that have been identified from their light curves.

I begin by compiling from the literature all known member stars, as well as the confirmed non-members, in each of these 17 systems. I only consider stars brighter than $g = 20$ because that is approximately where the *Gaia* DR2 proper motion accuracy reaches $\sim 1 \text{ mas yr}^{-1}$. I cross-match the spectroscopic catalogs against public photometric data from the Sloan Digital Sky Survey (SDSS; York et al. 2000) for dwarfs discovered in SDSS imaging, Pan-STARRS (Chambers et al. 2016) for dwarfs discovered in Pan-STARRS imaging, and the Dark Energy Survey (DES; Abbott et al. 2018) for dwarfs discovered in DES imaging. The most recently-found dwarfs (Carina II, Carina III, and Hydrus I) were identified in imaging surveys near the south celestial pole that are not currently public, so for those objects I use the coordinates and magnitudes provided in the discovery papers. Although the filters and photometric systems for SDSS, Pan-STARRS, and DECam are not identical, I do not

attempt to place the photometry on a common system, so the magnitudes reported here are heterogeneous at the level of a few percent.

In the Appendix I provide a detailed discussion of the sources of the spectroscopy and the size of the available member/non-member samples for each dwarf, in order of their right ascension. The assumed positions, distances, and velocities for the target galaxies are listed in Table 1.

3. VALIDATION

Because the *Gaia* DR2 data were just released, no independent checks of the astrometric performance in the regime of faint and distant sources are available yet. In this section I carry out some simple tests to assess the reliability of the dwarf galaxy proper motions I determine in Section 4. *Gaia* Collaboration et al. (2018c) find using an all-sky sample of quasars that on scales of $< 1^\circ$ there are systematics in the DR2 proper motions with a root-mean-square value of $0.066 \text{ mas yr}^{-1}$. They suggest that averaging of many faint sources cannot reduce the proper motion uncertainties below this floor. *Gaia* Collaboration et al. (2018b) use the largest dwarf galaxies on the sky, the Magellanic Clouds and Sagittarius, to provide an independent constraint on proper motion systematics and estimate an overall minimum systematic uncertainty of $\sim 0.035 \text{ mas yr}^{-1}$.

3.1. Ω Centauri

One of the most accurate extragalactic proper motions currently available is that determined by Libralato et al. (2018) for Ω Centauri. I query the *Gaia* DR2 catalog over a circle of radius $1.5'$ area centered on the coordinates of the Libralato et al. field, approximately matching their $2.73' \times 2.73'$ *HST* coverage.¹ As shown by Libralato et al. (2018), the foreground contamination in this region from Milky Way stars with proper motions similar to that of Ω Cen is quite small.

The stars in this field with *Gaia* proper motions broadly consistent with Ω Cen membership (within 10 mas yr^{-1} of that reported for Ω Cen by Libralato et al. 2018) have median proper motions of $\mu_\alpha \cos \delta = -3.26 \text{ mas yr}^{-1}$ and $\mu_\delta = -6.54 \text{ mas yr}^{-1}$. I select those stars with proper motions within 2 mas yr^{-1} of these values as the highest quality sample in this field. From the remaining 217 stars I determine a weighted average proper motion of $\mu_\alpha \cos \delta = -3.295 \pm 0.025 \text{ mas yr}^{-1}$, $\mu_\delta = -6.615 \pm 0.033 \text{ mas yr}^{-1}$. The *HST* proper motion in this field is $\mu_\alpha \cos \delta = -3.341 \pm 0.028 \text{ mas yr}^{-1}$, $\mu_\delta = -6.557 \pm 0.043 \text{ mas yr}^{-1}$. The *Gaia* and *HST* measurements agree at the $\sim 1\sigma$ level; if I included the systematic uncertainties listed above the agreement would be better than 1σ .

3.2. Leo I

The classical dSph with the most accurately measured proper motion is Leo I, with uncertainties of $\sim 0.03 \text{ mas yr}^{-1}$ per coordinate (Sohn et al. 2013). Leo I is a difficult target for *Gaia* because of its large distance (255 kpc; Held et al. 2001; Bellazzini et al. 2004), so that

¹ Although this area does not exactly match that of the *HST* pointing, given the large distance of this field from the center of Ω Cen, it is not important that an identical set of stars be used.

TABLE 1
ULTRA-FAINT DWARF POSITIONS, DISTANCES, AND VELOCITIES

Dwarf	R.A. (J2000) (deg)	Dec. (J2000) (deg)	Distance (kpc)	v_{hel} (km s $^{-1}$)	Position reference	Distance reference	Velocity reference
Triangulum II	33.3225	36.1783	30.0 \pm 2.0	-381.7 \pm 1.1	1	1	2
Segue 2	34.8167	20.1753	35.0 \pm 2.0	-40.2 \pm 0.9	3	3	4
Hydrus I	37.3890	-79.3089	27.6 \pm 0.5	80.4 \pm 0.6	5	5	5
Horologium I	43.8700	-54.1100	87.0 \pm 12.0	112.8 \pm 2.6	6	6	7
Reticulum II	53.9200	-54.0500	32.0 \pm 3.0	62.8 \pm 0.5	6	6	8
Carina II	114.1066	-57.9991	36.2 \pm 0.6	477.2 \pm 1.2	9	9	10
Carina III	114.6298	-57.8997	27.8 \pm 0.6	284.6 \pm 3.4	9	9	10
Ursa Major II	132.8744	63.1331	34.7 \pm 2.0	-116.5 \pm 1.9	11	12	13
Segue 1	151.7633	16.0736	23.0 \pm 2.0	208.5 \pm 0.9	14	15	16
Ursa Major I	158.6850	51.9261	97.3 \pm 6.0	-55.3 \pm 1.4	17	18	13
Willman 1	162.3413	51.0528	45.0 \pm 10.0	-12.8 \pm 1.0	14	19	20
Coma Berenices	186.7458	23.9076	42.0 \pm 2.0	98.1 \pm 0.9	11	21	13
Boötes II	209.5213	12.8586	42.0 \pm 2.0	-117.0 \pm 5.2	22	22	23
Boötes I	210.0225	14.5006	66.0 \pm 2.0	101.8 \pm 0.7	24	25	26
Draco II	238.1983	64.5653	20.0 \pm 3.0	-347.6 \pm 1.8	27	27	28
Tucana II	343.0600	-58.5700	58.0 \pm 8.0	-129.1 \pm 3.5	6	6	29
Tucana III	359.1500	-59.6000	25.0 \pm 2.0	-102.3 \pm 0.4	30	30	31

NOTE. — References: (1) Laevens et al. (2015a); (2) Kirby et al. (2017); (3) Belokurov et al. (2009); (4) Kirby et al. (2013a); (5) Koposov et al. (2018); (6) Bechtol et al. (2015); (7) Koposov et al. (2015a); (8) Simon et al. (2015); (9) Torrealba et al. (2018); (10) Li et al. (2018a); (11) Muñoz et al. (2010); (12) Dall’Ora et al. (2012); (13) Simon & Geha (2007); (14) Martin et al. (2008); (15) Belokurov et al. (2007); (16) Simon et al. (2011); (17) Okamoto et al. (2008); (18) Garofalo et al. (2013); (19) Willman et al. (2005); (20) Willman et al. (2011); (21) Musella et al. (2009); (22) Walsh et al. (2008); (23) Koch et al. (2009); (24) Okamoto et al. (2012); (25) Dall’Ora et al. (2006); (26) Koposov et al. (2011); (27) Laevens et al. (2015b); (28) Martin et al. (2016a); (29) Walker et al. (2016); (30) Drlica-Wagner et al. (2015); (31) Simon et al. (2017).

its proper motion is small and its brightest stars are at $V \approx 19$ (fainter than those in most of the ultra-faint dwarfs). On the other hand, it contains many more stars whose proper motions can be averaged together to reduce uncertainties. I select 202 Leo I members brighter than $V = 20$ from the spectroscopic catalog of Kirby et al. (2010). Of these, 187 stars have proper motions in the DR2 catalog, and the weighted average of this sample is $\mu_{\alpha} \cos \delta = -0.013 \pm 0.064$ mas yr $^{-1}$, $\mu_{\delta} = -0.091 \pm 0.066$ mas yr $^{-1}$. For comparison, Sohn et al. (2013) measure proper motions of $\mu_{\alpha} \cos \delta = -0.1140 \pm 0.0295$ mas yr $^{-1}$, $\mu_{\delta} = -0.1256 \pm 0.0293$ mas yr $^{-1}$. Because the Leo I stars are so faint the *Gaia* proper motion has larger uncertainties than those determined by *HST*. Still, the proper motion in declination agrees at better than 1σ , and that in right ascension differs by $\sim 1.4\sigma$ (again neglecting systematic uncertainties). Using a photometric DR2 sample rather than my spectroscopic one, Gaia Collaboration et al. (2018b) find $\mu_{\alpha} \cos \delta = -0.097 \pm 0.056$ mas yr $^{-1}$, $\mu_{\delta} = -0.091 \pm 0.047$ mas yr $^{-1}$, in agreement with my measurement within the uncertainties (see Figure 1).

3.3. Boötes I

My sample of ultra-faint dwarf galaxies has one object in common with that of Gaia Collaboration et al. (2018b): Boo I. Using a photometrically-selected sample as for Leo I, Gaia Collaboration et al. (2018b) measure proper motions of $\mu_{\alpha} \cos \delta = -0.459 \pm 0.041$ mas yr $^{-1}$, $\mu_{\delta} = -1.064 \pm 0.029$ mas yr $^{-1}$ from 115 stars. After rejecting 5 stars with deviant proper motions from the spectroscopic sample described in the Appendix, I measure $\mu_{\alpha} \cos \delta = -0.472 \pm 0.046$ mas yr $^{-1}$, $\mu_{\delta} = -1.086 \pm 0.034$ mas yr $^{-1}$ from 63 stars, in perfect agreement with Gaia Collaboration et al. (2018b) as shown in Fig. 1. The 5 astrometric non-members include: 3

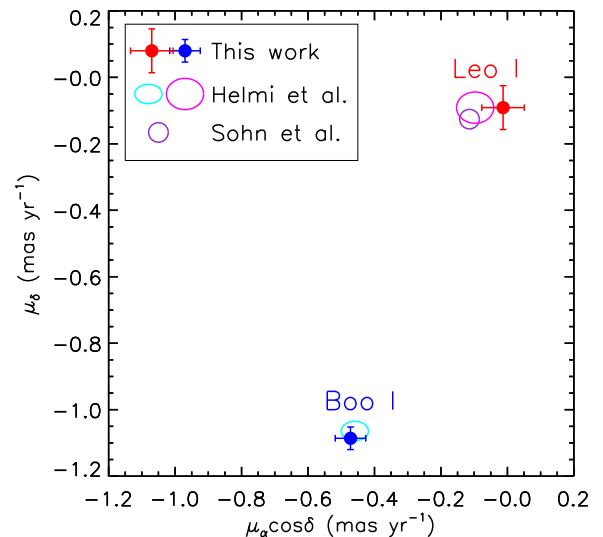


FIG. 1.— Comparison of my proper motion measurements with those of Gaia Collaboration et al. (2018b) for Leo I and Boo I. The solid points (red for Leo I and blue for Boo I) illustrate the proper motions I find in Sections 3.2 and 3.3, while the magenta (Leo I) and cyan (Boo I) ellipses represent the results from the *Gaia* collaboration. The purple circle for Leo I shows the *HST* measurement by Sohn et al. (2013).

stars at very large separations ($> 26'$) from Boo I from the sample of Norris et al. (2010b), one RRc variable $20'$ from the center of Boo I and with a similar mean magnitude to the other Boo I RR Lyrae but a larger photometric amplitude (Siegel 2006), and one star from Koposov et al. (2011) within the main body of Boo I but

with a radial velocity offset from the systemic velocity of the galaxy by $\sim 2\sigma$.

3.4. Background Quasars

Alternatively, instead of comparing the very small measured motions of stars by *Gaia* with the measured motions of similar stars from independent (but challenging) *HST* observations, one can check very distant extragalactic sources that can be assumed to be fixed on the sky. Of course, the *Gaia* team has already carried out extensive tests along these lines (e.g., Gaia Collaboration et al. 2018c). However, for completeness I perform this test in small areas around the ultra-faint dwarfs in case there are local systematic errors in any of these fields. I select spectroscopically-confirmed quasars from SDSS DR14 (Abolfathi et al. 2018) within $30'$ of each of the dwarfs within the SDSS footprint. Across the fields of 7 ultra-faint dwarfs (UMa II, Segue 1, UMa I, Willman 1, Com Ber, Boo II, and Boo I) I find a total of 154 SDSS quasars brighter than $g = 20$ that have counterparts in the *Gaia* DR2 catalog. The average proper motions in each field are consistent with a population of sources with zero net proper motion and Gaussian errors accurately described by the DR2 uncertainties. There is no evidence for a bias in *Gaia* proper motions near any of these dwarfs down to a level of $\sim 0.1 \text{ mas yr}^{-1}$. However, since the number of quasars in each field is small and the quasars are generally faint, this comparison is not sensitive to errors of the size of the estimated DR2 systematic uncertainties.

Based on the above comparisons with both an independent *Gaia* DR2 analysis and with *HST* data sets, I conclude that accurate DR2 proper motions can be straightforwardly measured for a number of extragalactic systems, and that any systematic uncertainties are comparable to or smaller than the statistical errors.

4. PROPER MOTIONS

For each of the ultra-faint dwarfs, I cross-match the confirmed member lists assembled in Section 2 with the *Gaia* DR2 catalog. I determine the proper motion of each system by taking a weighted average of the DR2 proper motions of the member stars. Because the uncertainties on these averages are already well above than the systematic error floor determined by Gaia Collaboration et al. (2018b) in most cases, I do not apply any additional correction to the derived uncertainties. In general, it is obvious from inspecting the distributions of proper motions for the known members, known non-members, and field stars that the member samples are free from contaminants and form tight distributions in proper motion space (see Figure 2). A catalog of the stars used in this analysis is provided in Table 2.

Even with only a handful of confirmed member stars in several of the target galaxies (e.g., Hyi 1, Car III, and Boo II), the proper motions are well-determined. By combining *Gaia* astrometry with standard color selection, identification of just a few bright members in a dwarf galaxy is sufficient to remove a very large fraction of the Milky Way foreground contamination for spectroscopic follow-up. I illustrate this process using Hyi I in Appendix R. Unsurprisingly, there are a few examples of stars that have been spectroscopically classified as ultra-faint dwarf members in the literature, but have proper

motions very different from those of the galaxies in which they supposedly reside. In particular, several of the spectroscopically-selected stars in Boo I are astrometric non-members (see Section 3.3), one UMa I star selected as a member by multiple authors has a proper motion of 32 mas yr^{-1} and must be a foreground main-sequence star, and one of the four published Hyi I members also appears unlikely to be associated with the galaxy based on its proper motion. I remove these stars with deviant proper motions before computing the weighted average.

The only system whose DR2 proper motions do not form an obvious kinematically coherent group is Segue 2 (see Figure 3). Two spectroscopic members of the Belokurov et al. (2009) stream have proper motions (which are different from each other) above 10 mas yr^{-1} , so I reject them as being associated with Segue 2. Even so, the remainder of the distribution is broader than seen for the other ultra-faint dwarfs. The 8 candidate stream stars without wildly deviant proper motions still exhibit a wide proper motion spread. Four stars form a separate tight group with $\mu_\alpha \cos \delta \sim 3 \text{ mas yr}^{-1}$, $\mu_\delta \sim -3 \text{ mas yr}^{-1}$ while the others are within or marginally outside the distribution of Segue 2 stars. These stars may be Segue 2 stars or field stars, but do not appear likely to be members of a stream given their significantly different proper motions. To be conservative, I exclude all of the stream candidates from the Segue 2 proper motion sample.

The proper motions and corresponding space velocities in the Cartesian Galactic frame² are presented in Table 3. The space velocities of the ultra-faint dwarfs are surprisingly large, exceeding 370 km s^{-1} with the exceptions of Segue 2, Willman 1, and Tuc III. The orbits are also almost exclusively retrograde with respect to Galactic rotation. Only Draco II and Tucana III have any significant motion in the direction of the rotation of the Milky Way disk. The vertical velocities are largely directed toward the north pole of the Galaxy, with the exceptions being Segue 1, UMa I, Boo II, and Dra II, most of which are located at high Galactic latitude. The kinematics of the UFD population are qualitatively similar to those of the Magellanic Clouds and Fornax, which also share positive W velocities and highly negative V velocities (Gaia Collaboration et al. 2018b). This suggests a possible association of many of these dwarfs with the Magellanic Clouds, as has been previously proposed (Deason et al. 2015; Jethwa et al. 2016; Sales et al. 2017).

5. SATELLITE ORBITS AROUND THE MILKY WAY

Using the proper motions determined with *Gaia* in Section 4 and positions and radial velocities from the literature, I calculate the orbit of each satellite around the Milky Way with the *galpy* software package (Bovy 2015). For simplicity and to maximize the reproducibility of the results, I use the recommended MWPotential2014 gravitational potential for the Milky Way with its default parameters ($R_0 = 8.0 \text{ kpc}$, $V_0 = 220 \text{ km s}^{-1}$); I note that there is not currently compelling observational evidence to favor the adoption of a different potential. I

² The sign conventions I use are that U velocities are positive toward the Galactic anticenter, V velocities are positive in the direction of Galactic rotation, and W velocities are positive toward the north pole of the Milky Way. Note that this convention for U is opposite to that chosen by Gaia Collaboration et al. (2018b).

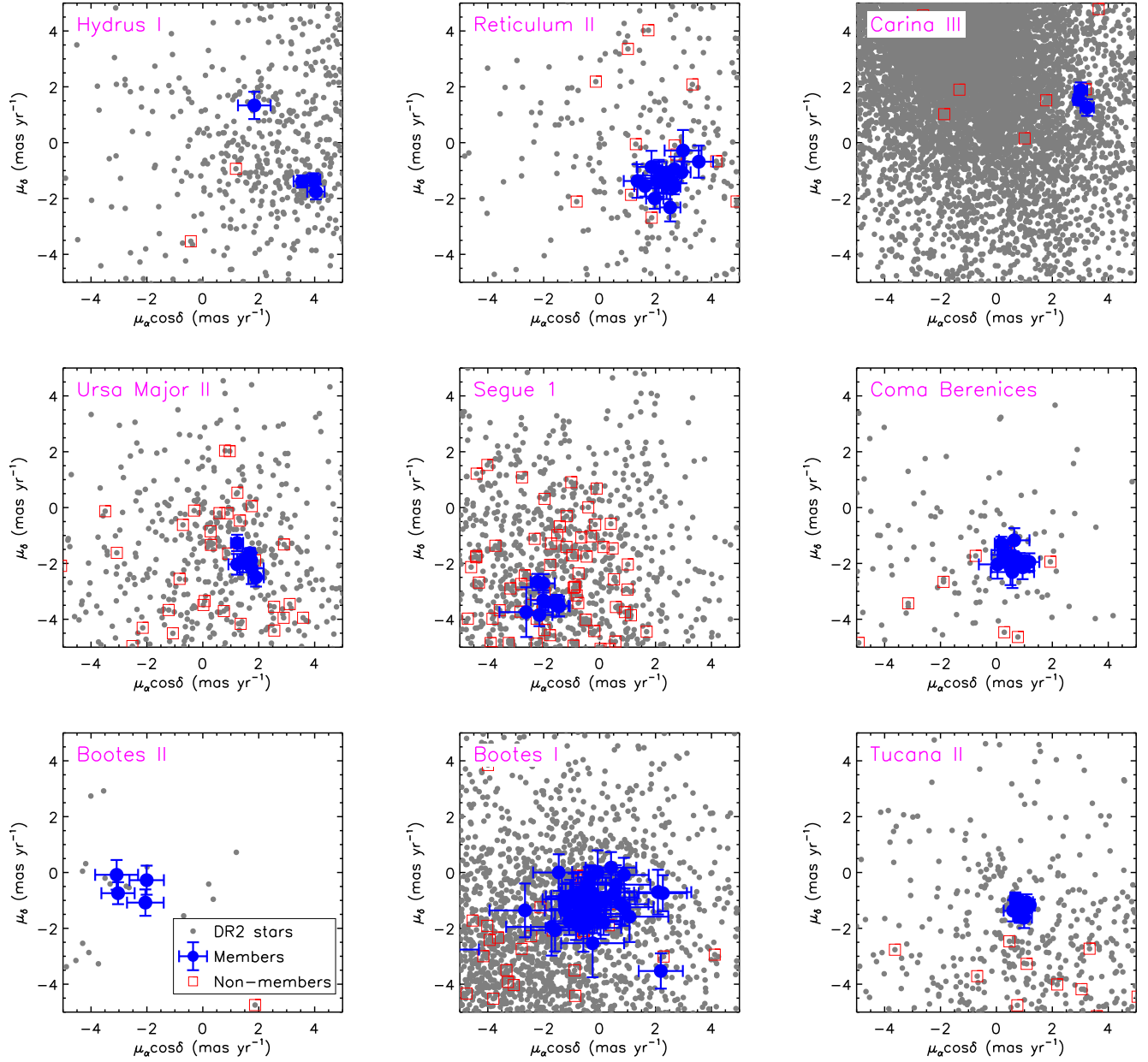


FIG. 2.— *Gaia* DR2 proper motion diagrams of a subset of the target galaxies. The area over which stars are selected from the DR2 catalog varies from galaxy to galaxy depending on the extent of the spectroscopic coverage; stars are selected out to a radius just beyond the most distant confirmed members/non-members. All stars in the field are plotted as small gray dots, member stars are shown as blue circles, and spectroscopic non-members are plotted as red squares. Even for objects with very small spectroscopic samples such as Hyi I, Car III, and Boo II it is clear that the members exhibit coherent proper motions that are distinct from those of other stars in the field.

assume the solar motion determined by Schönrich et al. (2010) throughout this paper.

Because the observational uncertainties on the proper motions and distances are large in some cases (see Tables 1 and 3), I calculate orbits by drawing 1000 random proper motion, distance and radial velocity values from Gaussian distributions. The Gaussian distributions are defined such that the mean is the measured value of that parameter, and the standard deviation is equal to the 1σ observational uncertainty. I recompute the orbit for each of the 1000 parameter sets and take the 16th, 50th, and 84th percentiles of the resulting distributions to describe the median and 1σ confidence interval of the orbit.

Uncertainties on the central positions of the ultra-faint dwarfs have only been published for about half of the objects included in my sample. The typical positional uncertainties for the systems for which they have been reported are $\sim 0.003^\circ$ ($\sim 11''$) per coordinate. These uncertainties impart negligible changes to the orbits, so I ignore them. I report the derived orbital pericenters, apocenters, eccentricities, and periods in Table 4, and projections of the orbits are shown in Figures 5 and 6.

In addition to Boo I (Section 3.3), the other ultra-faint dwarf with a literature proper motion measurement is Segue 1. Fritz et al. (2017) determined a proper motion of $\mu_\alpha \cos \delta = -0.37 \pm 0.57 \text{ mas yr}^{-1}$,

TABLE 2
Gaia DR2 PROPER MOTIONS OF STARS IN ULTRA-FAINT DWARF GALAXIES

ID	Dwarf	R.A. (deg)	Dec. (deg)	g	r	$\mu_\alpha \cos \delta$ (mas yr ⁻¹)	μ_δ (mas yr ⁻¹)	References ^a	Comment
PS1J02131655+3610458	Tri II	33.31894	36.17938	17.60	17.01	0.406 ± 0.209	0.511 ± 0.176	1,2,3,4	
PS1J02132154+3609574	Tri II	33.33976	36.16594	19.29	18.81	2.044 ± 0.499	1.093 ± 0.439	1,2,3,4	
SDSSJ02191849+2010219	Segue 2	34.82706	20.17275	18.76	18.81	2.327 ± 0.818	1.253 ± 0.753	5,6	
SDSSJ02192430+2010168	Segue 2	34.85125	20.17133	18.93	18.19	1.060 ± 0.520	-0.813 ± 0.316	5,6	
SDSSJ02190759+2012209	Segue 2	34.78161	20.20578	18.84	18.78	0.805 ± 0.926	0.085 ± 0.498	5,6	
SDSSJ02190493+2007154	Segue 2	34.77053	20.12095	19.98	19.24	1.182 ± 0.883	0.758 ± 0.597	5,6	
SDSSJ02190004+2009457	Segue 2	34.75018	20.16270	19.60	18.84	0.452 ± 0.622	-0.956 ± 0.431	5,6	
SDSSJ02193468+2011443	Segue 2	34.89448	20.19565	19.25	19.34	2.007 ± 1.254	-1.753 ± 0.658	5,6	
SDSSJ02192271+2004433	Segue 2	34.84463	20.07870	19.55	18.81	2.163 ± 0.626	0.233 ± 0.508	5,6	
SDSSJ02195535+2007492	Segue 2	34.98061	20.13034	19.18	18.49	2.660 ± 0.668	0.023 ± 0.352	5,6	
SDSSJ02190006+2006351	Segue 2	34.75026	20.10978	19.16	18.61	1.309 ± 0.521	-0.895 ± 0.396	6,7	
SDSSJ02191711+2009306	Segue 2	34.82127	20.15849	19.84	19.20	3.492 ± 0.941	1.022 ± 0.963	6	
SDSSJ02193313+2008302	Segue 2	34.88806	20.14173	17.19	16.19	1.694 ± 0.188	0.128 ± 0.121	6,8	
DECJ02305767-7921156	Hy I	37.74031	-79.35435	19.03	18.44	4.044 ± 0.312	-1.755 ± 0.276	9	
DECJ02311155-7924240	Hy I	37.79813	-79.40667	19.81	19.29	1.841 ± 0.583	1.334 ± 0.487	9	PM non-member
OGL4J02294391-7916384	Hy I	37.43306	-79.27732	18.00	17.35	3.963 ± 0.236	-1.320 ± 0.223	9	
OGL4J02323035-7927272	Hy I	38.12667	-79.45753	17.99	17.31	3.545 ± 0.298	-1.387 ± 0.216	9	

NOTE. — This table is available in its entirety in the electronic edition of the journal. A portion is reproduced here to provide guidance on form and content.

^a References: (1) Kirby et al. (2015); (2) Martin et al. (2016b); (3) Kirby et al. (2017); (4) Venn et al. (2017); (5) Belokurov et al. (2009); (6) Kirby et al. (2013a); (7) Boettcher et al. (2013); (8) Roederer & Kirby (2014); (9) Koposov et al. (2018); (10) Koposov et al. (2015b); (11) Nagasawa et al. (2018); (12) Simon et al. (2015); (13) Ji et al. (2016a); (14) Ji et al. (2016c); (15) Roederer et al. (2016); (16) Ji & Frebel (2018); (17) Li et al. (2018a); (18) Torrealba et al. (2018); (19) Martin et al. (2007); (20) Simon & Geha (2007); (21) Frebel et al. (2010); (22) Dall’Ora et al. (2012); (23) Geha et al. (2009); (24) Norris et al. (2010b); (25) Norris et al. (2010a); (26) Simon et al. (2011); (27) Frebel et al. (2014); (28) Kleyna et al. (2005); (29) Brown et al. (2014); (30) Siegel et al. (2008); (31) Willman et al. (2011); (32) Musella et al. (2009); (33) Koch et al. (2009); (34) Koch & Rich (2014); (35) Ji et al. (2016d); (36) François et al. (2016); (37) Muñoz et al. (2006); (38) Siegel (2006); (39) Feltzing et al. (2009); (40) Norris et al. (2010c); (41) Koposov et al. (2011); (42) Lai et al. (2011); (43) Gilmore et al. (2013); (44) Ishigaki et al. (2014); (45) Frebel et al. (2016); (46) Martin et al. (2016a); (47) Walker et al. (2016); (48) Ji et al. (2016b); (49) Chiti et al. (2018); (50) Simon et al. (2017); (51) Hansen et al. (2017);

TABLE 3
GAIA DR2 PROPER MOTIONS AND SPACE VELOCITIES

Dwarf	N _{stars}	$\mu_\alpha \cos \delta$ (mas yr ⁻¹)	μ_δ (mas yr ⁻¹)	U (km s ⁻¹)	V (km s ⁻¹)	W (km s ⁻¹)
Triangulum II	2	0.651 ± 0.193	0.592 ± 0.164	-199.4	-237.4	255.4
Segue 2	11	1.650 ± 0.143	-0.065 ± 0.094	157.6	-200.3	108.2
Hydrus I	3	3.865 ± 0.159	-1.450 ± 0.135	180.4	-436.8	273.6
Horologium I	6	0.901 ± 0.070	-0.583 ± 0.067	24.5	-426.1	162.6
Reticulum II	22	2.393 ± 0.040	-1.300 ± 0.048	-0.6	-356.1	218.6
Carina II	19	1.886 ± 0.076	0.079 ± 0.070	-119.1	-544.8	147.1
Carina III	3	3.035 ± 0.120	1.558 ± 0.136	21.3	-402.5	347.3
Ursa Major II	8	1.661 ± 0.053	-1.870 ± 0.065	-157.2	-344.6	198.5
Segue 1	9	-1.867 ± 0.110	-3.282 ± 0.102	132.7	-439.3	-48.7
Ursa Major I	8	-0.659 ± 0.093	-0.635 ± 0.131	197.3	-361.0	-109.5
Willman 1	4	0.382 ± 0.119	-1.152 ± 0.216	-109.8	-211.4	102.2
Coma Berenices	12	0.546 ± 0.092	-1.726 ± 0.086	-262.3	-251.0	87.8
Boötes II	4	-2.517 ± 0.325	-0.602 ± 0.235	340.0	-404.3	-11.8
Boötes I	68	-0.472 ± 0.046	-1.086 ± 0.034	-128.2	-357.8	56.6
Draco II	4	1.170 ± 0.297	0.871 ± 0.303	-8.0	-161.7	-337.2
Tucana II	10	0.936 ± 0.057	-1.232 ± 0.072	259.0	-336.7	131.1
Tucana III	10	-0.014 ± 0.038	-1.673 ± 0.040	-16.6	-119.8	187.5

$\mu_\delta = -3.39 \pm 0.58$ mas yr⁻¹ using ground-based data over a time baseline of 10 years. The DR2 measurement has uncertainties smaller by a factor of ~ 5 and is in excellent agreement in the Declination direction, but the motions in Right Ascension differ by 2.6σ . Nevertheless, the derived orbits are quite similar, with overlapping pericenter and apocenter ranges. Although the proper motion of Tuc III has not previously been measured, Erkal et al. (2018) predicted its proper motion based on the stellar kinematics of its tidal tails provided by Li et al. (2018b). The properties of the Tuc III orbit such as its eccentricity and pericenter, as well as the μ_δ value, are close to the Erkal et al. prediction, but the proper motion in $\mu_\alpha \cos \delta$ is much closer to zero than expected. Exploration of the

Tuc III orbit in different gravitational potentials for the Milky Way and the LMC may be required to understand this discrepancy.

The pericentric distances of the ultra-faint dwarfs are tightly constrained by the *Gaia* proper motions, with typical uncertainties of 5 kpc. The best-fit pericenter is beyond 20 kpc for every galaxy except Tuc III, which approaches within 3 kpc of the Galactic Center. Not surprisingly given this extreme orbit, Tuc III has been tidally disrupted, with obvious tidal tails in DES imaging (Drlica-Wagner et al. 2015; Shipp et al. 2018) and a kinematic gradient detected along the tails (Li et al. 2018b; Erkal et al. 2018). None of the other dwarfs have orbits that penetrate significantly into the disk or bulge.

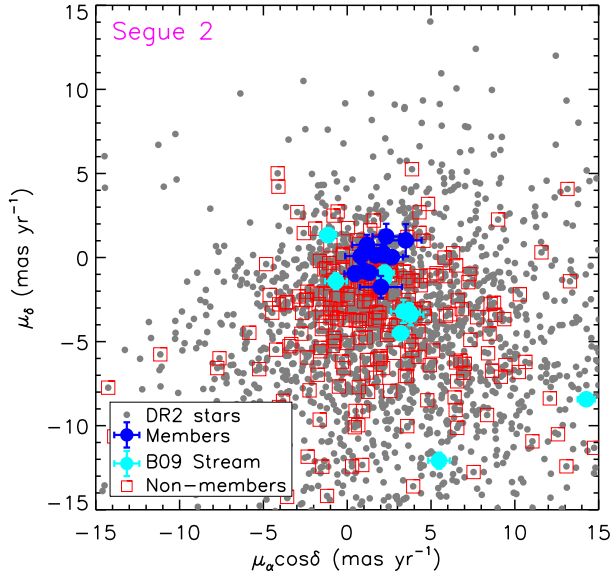


FIG. 3.— Proper motion diagram for Segue 2. Symbols are as in Figure 2, with the exception of the cyan points, which represent members of the stream identified by Belokurov et al. (2009).

TABLE 4
ORBITS

Dwarf	Pericenter (kpc)	Apocenter (kpc)	Eccentricity	Period (Gyr)
Triangulum II	20^{+2}_{-3}	541^{+493}_{-211}	$0.93^{+0.03}_{-0.03}$	>10
Segue 2	32^{+4}_{-5}	54^{+14}_{-7}	$0.32^{+0.62}_{-0.04}$	1.1
Hydrus I	26^{+1}_{-1}	1029^{+642}_{-610}	$0.95^{+0.02}_{-0.06}$	>10
Horologium I	87^{+12}_{-15}	741^{+1331}_{-619}	$0.79^{+0.12}_{-0.50}$...
Reticulum II	29^{+4}_{-6}	91^{+91}_{-39}	$0.51^{+0.18}_{-0.13}$	1.6
Carina II	28^{+1}_{-1}	1521^{+232}_{-231}	$0.96^{+0.01}_{-0.01}$	>10
Carina III	29^{+1}_{-1}	1478^{+436}_{-488}	$0.96^{+0.01}_{-0.02}$	>10
Ursa Major II	39^{+2}_{-3}	201^{+179}_{-80}	$0.67^{+0.13}_{-0.14}$	3.5
Segue 1	20^{+4}_{-5}	61^{+34}_{-18}	$0.52^{+0.08}_{-0.03}$	1.1
Ursa Major I	102^{+6}_{-7}	896^{+937}_{-669}	$0.79^{+0.1}_{-0.39}$...
Willman 1	44^{+15}_{-19}	53^{+57}_{-13}	$0.19^{+0.19}_{-0.11}$	1.2
Coma Berenices	43^{+2}_{-2}	242^{+192}_{-87}	$0.70^{+0.12}_{-0.12}$	3.7
Boötes II	39^{+2}_{-2}	1746^{+1439}_{-1120}	$0.96^{+0.02}_{-0.17}$	>10
Boötes I	45^{+5}_{-5}	116^{+21}_{-15}	$0.44^{+0.03}_{-0.01}$	2.4
Draco II	18^{+3}_{-3}	158^{+255}_{-71}	$0.79^{+0.11}_{-0.10}$	2.0
Tucana II	39^{+12}_{-12}	626^{+1654}_{-449}	$0.78^{+0.16}_{-0.09}$...
Tucana III	3^{+1}_{-1}	49^{+6}_{-5}	$0.90^{+0.01}_{-0.01}$	0.7

Strikingly, a large majority of these dwarfs are currently located very close to the pericenters of their orbits around the Milky Way. Whether this result can be attributed to observational selection effects or other factors is not yet clear.

Under the assumption that the mass distribution of the Milky Way follows that of the MWPotential2014 model, nearly half of the target galaxies lack well-determined orbital apocenters, and they appear likely to be on their first orbit around the Milky Way. However, the MWPotential2014 mass model corresponds to a relatively low-mass Milky Way of $M_{\text{vir}} = 0.8 \times 10^{12} M_{\odot}$ (Bovy 2015). The large fraction of objects apparently on their first infall to the Milky Way when their orbits are integrated in this potential suggests that the mass of the Milky Way

might be underestimated in this model. To test this idea, I recomputed orbits for the eight dwarfs with very large apocenters in the extreme case of a Milky Way circular velocity of 250 km s^{-1} , compared to the assumed value of 220 km s^{-1} . With this more massive potential, seven of the eight first-infall objects have orbital apocenters of less than 300 kpc and typical periods of 2 – 4 Gyr. In some fraction of the Monte Carlo iterations these dwarfs are still on their first infall, but such orbits become a minority of those simulated. The only exception is Boo II, which still has an apocenter of 482^{+1592}_{-347} kpc in this potential and is on its first infall.

6. DISCUSSION

6.1. Tidal Stripping of the Ultra-Faint Dwarfs

Since shortly after their initial discovery, it has frequently been speculated that many ultra-faint dwarfs are heavily tidally stripped systems (e.g., Niederste-Ostholt et al. 2009; Martin & Jin 2010; Muñoz et al. 2010; Sand et al. 2012; Kirby et al. 2013a; Roderick et al. 2015, 2016; Collins et al. 2017; Garling et al. 2018). On the other hand, Peñarrubia et al. (2008) showed using N-body simulations that the properties of the ultra-faint dwarfs did not seem to be consistent with being the tidally-stripped remnants of the classical dSphs. The existence of a mass-metallicity relationship extending down to the lowest luminosity dwarfs is also inconsistent with the idea that many of the ultra-faint dwarfs have been significantly stripped (Kirby et al. 2013b). However, only orbital measurements can show conclusively whether these systems have been subject to strong enough tidal forces to remove many of their stars. For Tuc III, the answer is unequivocally yes, as shown by its orbit derived here and the studies of Li et al. (2018b) and Erkal et al. (2018). The other dwarfs in my sample, though, remain well away from the regions where the Milky Way’s tidal field is strongest. After Tuc III, the next closest orbital pericenters are those of Segue 1 and Tri II, each at 20 kpc. Using the mass determined from the internal kinematics of its stars, Simon et al. (2011) showed that the tidal radius of Segue 1 remains well beyond its stellar distribution unless the galaxy has an orbital pericenter of ~ 4 kpc or less. My results here show that Segue 1 cannot have experienced significant stellar stripping (also see Fritz et al. 2017 for independent confirmation). The same is likely true for most of the rest of the ultra-faint dwarf population. While the dark matter halos of these galaxies, which extend to much larger radii than the stars, may suffer substantial tidal effects, the stars at the center of the halo are protected from the influence of Galactic tides.

6.2. Comparison to Predicted Proper Motions

Several recent studies have provided predictions for the proper motions of the ultra-faint dwarfs, based either on the possibility that they are distributed in a thin, rotating vast polar structure (VPOs; Pawlowski & Kroupa 2013; Pawlowski et al. 2015) or that they were accreted as members of a Magellanic group of dwarf galaxies (Jethwa et al. 2016; Sales et al. 2017). The results of the Pawlowski & Kroupa (2013) and Pawlowski et al. (2015) predictions are mixed: several satellites are consistent with being co-rotating with the polar structure

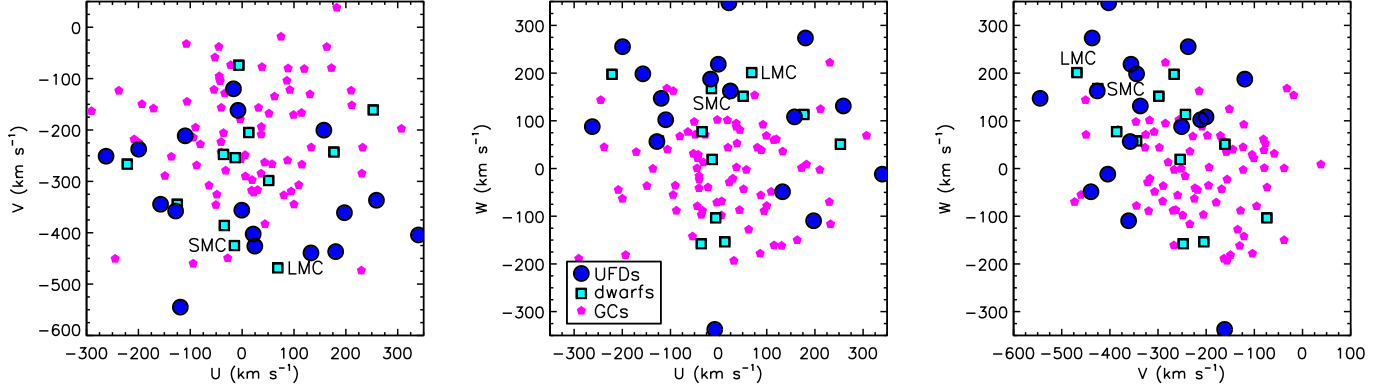


FIG. 4.— UVW velocities for ultra-faint dwarfs (blue circles), more luminous dwarfs (cyan squares), and globular clusters (magenta pentagons). The motions of the luminous dwarfs and globular clusters are taken from Gaia Collaboration et al. (2018b), adjusted for the different sign convention for U that I use. The ultra-faint dwarfs are preferentially moving on retrograde orbits with positive vertical velocities, similar to the Magellanic Clouds. The LMC $(U, V, W) = (68.6, -468.4, 201.0)$ and SMC $(U, V, W) = (-14.8, -425.0, 167.5)$ are labeled in each panel.

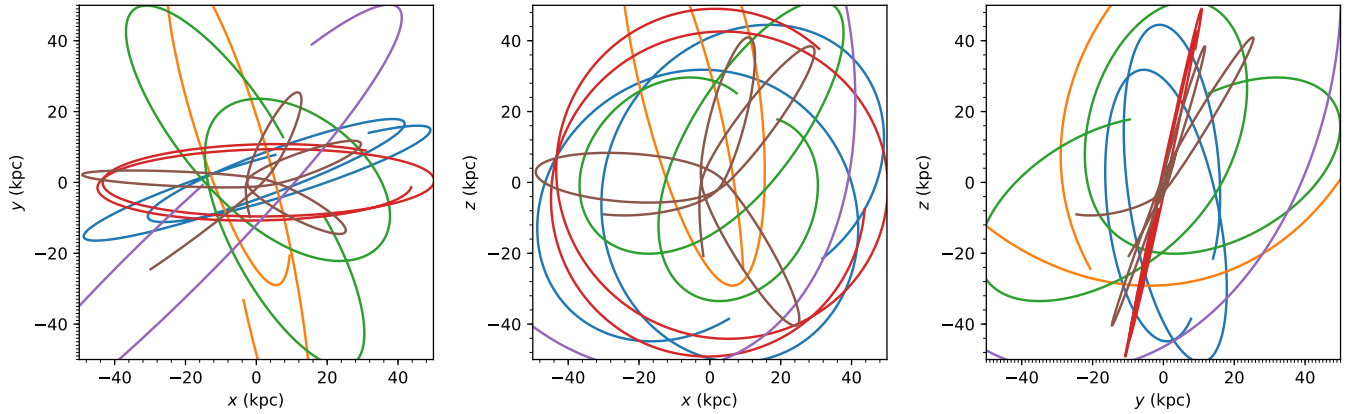


FIG. 5.— (left) Projections of the orbits on the X-Y plane for the ultra-faint dwarfs that are confined to Galactocentric radii of less than 100 kpc. (middle) Projections of the orbits on the X-Z plane for the same dwarfs. (right) Projections of the orbits on the Y-Z plane. Segue 2 is plotted as the blue curve, Ret II is orange, Segue 1 is green, Willman 1 is red, Boo I is purple, and Tuc III is brown. The orbits are integrated for 4 Gyr.

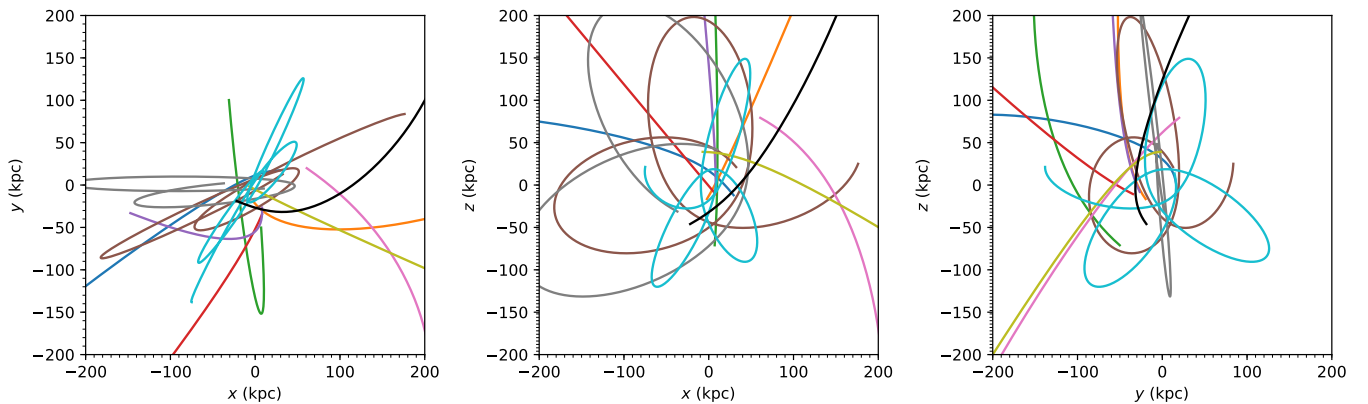


FIG. 6.— (left) Projections of the orbits on the X-Y plane for the ultra-faint dwarfs with orbits that extend beyond 200 kpc. (middle) Projections of the orbits on the X-Z plane for the same dwarfs. (right) Projections of the orbits on the Y-Z plane. Tri II is plotted as the blue curve, Hyi I is orange, Hor I is green, Car II is red, Car III is purple, UMa II is brown, UMa I is pink, Com Ber is gray, Boo II is chartreuse, Dra II is cyan, and Tuc II is black. The orbits are integrated for 10 Gyr.

(Hor I, Ret II, Willman 1, and Tuc II), Segue 1 is counter-rotating, and four other dwarfs (UMa II, Com Ber, Boo II, and Boo I) are outside the expected proper motion ranges. Moreover, the orbit integrations shown in

Figures 5 and 6 indicate that the population as a whole is not confined to a thin plane, consistent with the results of Gaia Collaboration et al. (2018b) for the more luminous dwarf galaxies.

Jethwa et al. (2016) provide predictions for the proper motions of four of the targets of this study under the assumption that they originated as satellites of the Magellanic Clouds. As noted earlier, there are qualitative resemblances between many of the orbits I derive and those of the Magellanic Clouds. Hor I and Ret II have proper motions in the right ascension direction in agreement with the Jethwa et al. predictions, but the motions in declination are inconsistent with the predicted values at the $2 - 3\sigma$ level. For Tuc II, the opposite is the case: the proper motion in declination is marginally consistent with the prediction, but the proper motion in R.A. is not. The predicted ranges for Tuc III are so wide that the satellite was virtually guaranteed to fall within them. These four objects, as well as Hyi I, Car II, and Car III, all of which were discovered too recently for predictions to be available, can be regarded as candidate Magellanic satellites. Viewed in three dimensions and integrated backward in time, the orbits of Hor I, Hyi I, Car III, and Tuc II track that of the LMC quite closely, suggesting that these objects are probably associated with the Magellanic system. Deason et al. (2015) and Sales et al. (2017) both consider Hor I and Tuc II to be the most likely dwarfs of Magellanic origin, which is consistent with the results reported here.

6.3. Comparison to Numerical Simulations

N-body simulations of dark matter halo formation in the Λ CDM paradigm show that subhalos are usually on quite radial orbits, with typical pericenter to apocenter ratios of ~ 0.2 (e.g., van den Bosch et al. 1999; Diemand et al. 2007; Wetzel 2011; Barber et al. 2014). Contrary to this expectation, Gaia Collaboration et al. (2018b) find that the orbits of the classical dSphs are relatively round, with the exceptions of the most distant objects, Leo I and Leo II. On the other hand, the results presented here are very consistent with the predicted orbital distribution, with eccentricities exceeding 0.9 for more than a third of the sample. The large eccentricities I measure may be connected to the preference for first-infall orbits discussed in Section 5; Gill et al. (2004) showed that satellite orbits tend to get rounder as their time within the host halo increases.

It is worth noting that the N-body results may not represent an accurate prediction for what should be observed. In simulations including hydrodynamics, many of the subhalos that approach within 30 kpc of the center of their host galaxy are destroyed by tidal interactions (Garrison-Kimmel et al. 2017; Sawala et al. 2017). In that respect, it may be unexpected that so many of the dwarfs have orbital pericenters of less than 30 kpc. However, because their orbits are so eccentric they spend very little time in the central regions of the Milky Way, enabling them to survive until the present (Sawala et al. 2017). More detailed work on the predicted distribution of subhalo orbits when baryonic physics is included in simulations would be fruitful now that there is a significant set of observations with which to compare.

6.4. Infall Times

Rocha et al. (2012) showed that there is a strong correlation between the binding energy of a subhalo and the time it was accreted by the host halo. Using Eq. 1 from

their paper, I calculate the binding energies for the 17 ultra-faint dwarfs studied here. For the majority of the sample the binding energy defined in this way is negative and the Rocha et al. (2012) analysis does not apply. This result is obviously related to the apparent first-infall status of many of these galaxies. Among the galaxies for which the binding energy is well-behaved, the Rocha et al. (2012) relation suggests infall times of ~ 7 Gyr for Tri II, Segue 2, and Willman 1, ~ 8 Gyr for Draco II and Tuc III, and > 12 Gyr for Ret II. Ret II has a higher binding energy than any of the Via Lactea 2 subhalos included in the Rocha et al. sample.

6.5. Implications for the Mass of the Milky Way

As discussed in previous sections and shown in Figure 6, a number of the target galaxies of this study appear to be very loosely bound and may be on their first orbital passage around the Milky Way, which would be an unexpected result. I showed in Section 5 that this problem can be alleviated if the mass of the Milky Way is larger than assumed in the default `galpy` MWPotential2014 model. Relatively large Milky Way masses have been advocated by some authors (e.g., Boylan-Kolchin et al. 2013), but if the mass of the Galaxy is large that will tend to exacerbate issues such as the missing satellite problem (Klypin et al. 1999; Moore et al. 1999) and the too big to fail problem (Boylan-Kolchin et al. 2011, 2012).

The alternative explanation is that many of the ultra-faint satellites are on their first orbit because they formed in a Magellanic group that is now infalling into the Milky Way for the first time (Besla et al. 2007; Kallivayalil et al. 2013). However, if many of the currently known satellites were originally located around the LMC, that also has adverse consequences for the missing satellite problem, because the number of dwarfs formed around the Milky Way would be even smaller. Improved estimates of the Milky Way’s mass based on dynamical modeling of the kinematics of the satellite population provided here and by Gaia Collaboration et al. (2018b) will be valuable for attempting to resolve this dilemma.

7. SUMMARY AND CONCLUSIONS

I have presented *Gaia* DR2-based proper motions, space velocities, and Galactic orbits for 17 ultra-faint satellites of the Milky Way. I cross-match lists of member stars that are confirmed via spectroscopy or variable star pulsations with the *Gaia* DR2 catalog to determine the motion of each system across the sky. Thanks to the exquisite astrometric performance of *Gaia*, even with as few as ~ 3 member stars brighter than $g = 20$ per satellite, the proper motions are determined with a typical precision of ~ 0.1 mas yr $^{-1}$ per coordinate. At a median distance of 35 kpc, the uncertainties on the tangential velocities are therefore ~ 25 km s $^{-1}$. I find good agreement with the proper motion measurements reported by Gaia Collaboration et al. (2018b) for Boötes I and Leo I, as well as with *HST* measurements of Leo I (Sohn et al. 2013) and Ω Centauri (Libralato et al. 2018).

The tangential velocities of the sample of ultra-faint dwarfs analyzed here are generally much larger than the line-of-sight velocities measured in the literature, with a median value exceeding 400 km s $^{-1}$. Most of the dwarfs are orbiting in the opposite direction from the rotation

of the Milky Way and are moving toward the northern hemisphere of the Galaxy, broadly similar to the space motions of the Magellanic Clouds. I use `galpy` (Bovy 2015) to integrate the orbits of the ultra-faint dwarfs in the potential of the Milky Way. The resulting orbital parameters are surprising in a number of related ways:

- The dwarfs are moving at very high velocities. The tangential velocities are significantly higher than the radial velocities for 14 out of the 17 dwarfs.
- A large fraction of the satellites are currently located near the pericenters of their orbits. More than half of the sample (Hyi I, Hor I, Ret II, Car III, UMa II, UMa I, Com Ber, Boo II, and Dra II) is within 4 kpc of the derived pericenter, and most of the satellites are no more than 100 Myr away from passing or reaching pericenter.
- The orbital eccentricities are very high, comparable to those found in pure dark matter N-body simulations, but significantly larger than those of the classical dwarf spheroidals (Gaia Collaboration et al. 2018b). Only Willman 1 is robustly on a circular orbit; the orbit of Segue 2 is consistent with being relatively round but with large uncertainties. Segue 1 and Boo I have orbital eccentricities of ~ 0.5 , and the remainder of the sample has eccentricities ranging from 0.67 to 0.96.
- If the recommended `galpy` gravitational potential for the Milky Way is used, many of the ultra-faint dwarfs have orbital apocenters well beyond the virial radius of the Milky Way and have yet to complete a single orbit around the Galaxy. A larger mass for the Milky Way can bring the derived apocenters down to more reasonable values (with the exception of Boo II), at the cost of worsening other problems in near-field cosmology and increasing tension with a variety of evidence for a relatively low-mass Milky Way. Alternatively, perhaps more of these satellites than expected have been stripped from the Magellanic system.

Of the galaxies considered in this paper, only the tidally disrupting Tuc III system has an orbital pericenter of less than 20 kpc. Because of their eccentric orbits and large pericentric distances, the stellar components of the other dwarfs likely have not been significantly affected by Galactic tides.

Predictions for the proper motions of a number of the dwarfs studied here have been made in the literature, assuming either that they are orbiting within a vast polar structure (Pawlowski & Kroupa 2013; Pawlowski et al. 2015) or that they were accreted by the Milky Way from the Magellanic Clouds (Jethwa et al. 2016; Sales et al. 2017). A portion of the sample has velocities that are consistent with the VPOS predictions, but other objects do not, and the orbits of the full sample are not primarily confined to a thin plane. Several of the southern dwarfs, such as Hyi I, Hor I, Car III, and Tuc II, have orbits suggesting that they are (or were) Magellanic satellites.

The *Gaia* DR2 data represent such an enormous step forward in size, depth, and astrometric accuracy that the analysis I present here only scratches the surface of

what is now possible. *Gaia* measurements can likely be obtained for additional dwarf galaxies, bringing the dynamics of the Milky Way’s entire surroundings into sharp focus for the first time. The measured proper motions for many of the dwarfs studied here can also be improved by obtaining larger spectroscopic (or photometric) member samples, and the efficiency of spectroscopic target selection will be greatly enhanced by the availability of *Gaia* astrometry once the approximate proper motion of any nearby dwarf is known. I look forward to these and many other foreseen and unforeseen results in the near future. The *Gaia* revolution has begun!

I thank Marla Geha, Juna Kollmeier, Sal Fu, Ting Li, Jo Bovy, Alex Ji, Andrew Wetzel, and Denis Erkal for helpful conversations. I also thank the entire *Gaia* collaboration for their hard work in producing this astonishing data set. This publication is based upon work supported by the National Science Foundation under grant AST-1714873. Assemblage of the spectroscopic samples for some of the dwarf galaxies included here was supported by a NASA Keck PI Data Award, administered by the NASA Exoplanet Science Institute under RSA number 1474359. This research has made use of NASA’s Astrophysics Data System Bibliographic Services.

This work has made use of data from the European Space Agency (ESA) mission *Gaia* (<https://www.cosmos.esa.int/gaia>), processed by the *Gaia* Data Processing and Analysis Consortium (DPAC, <https://www.cosmos.esa.int/web/gaia/dpac/consortium>). Funding for the DPAC has been provided by national institutions, in particular the institutions participating in the *Gaia* Multilateral Agreement.

This publication made use of data from the Sloan Digital Sky Survey. Funding for SDSS-III has been provided by the Alfred P. Sloan Foundation, the Participating Institutions, the National Science Foundation, and the U.S. Department of Energy Office of Science. The SDSS-III web site is <http://www.sdss3.org/>.

SDSS-III is managed by the Astrophysical Research Consortium for the Participating Institutions of the SDSS-III Collaboration including the University of Arizona, the Brazilian Participation Group, Brookhaven National Laboratory, Carnegie Mellon University, University of Florida, the French Participation Group, the German Participation Group, Harvard University, the Instituto de Astrofísica de Canarias, the Michigan State/Notre Dame/JINA Participation Group, Johns Hopkins University, Lawrence Berkeley National Laboratory, Max Planck Institute for Astrophysics, Max Planck Institute for Extraterrestrial Physics, New Mexico State University, New York University, Ohio State University, Pennsylvania State University, University of Portsmouth, Princeton University, the Spanish Participation Group, University of Tokyo, University of Utah, Vanderbilt University, University of Virginia, University of Washington, and Yale University.

This project used public archival data from the Dark Energy Survey (DES). Funding for the DES Projects has been provided by the U.S. Department of Energy, the U.S. National Science Foundation, the Ministry of Science and Education of Spain, the Science and Technol-

ogy Facilities Council of the United Kingdom, the Higher Education Funding Council for England, the National Center for Supercomputing Applications at the University of Illinois at Urbana-Champaign, the Kavli Institute of Cosmological Physics at the University of Chicago, the Center for Cosmology and Astro-Particle Physics at the Ohio State University, the Mitchell Institute for Fundamental Physics and Astronomy at Texas A&M University, Financiadora de Estudos e Projetos, Fundação Carlos Chagas Filho de Amparo à Pesquisa do Estado do Rio de Janeiro, Conselho Nacional de Desenvolvimento Científico e Tecnológico and the Ministério da Ciência, Tecnologia e Inovação, the Deutsche Forschungsgemeinschaft, and the Collaborating Institutions in the Dark Energy Survey.

The Collaborating Institutions are Argonne National Laboratory, the University of California at Santa Cruz, the University of Cambridge, Centro de Investigaciones Energéticas, Medioambientales y Tecnológicas-Madrid, the University of Chicago, University College London, the DES-Brazil Consortium, the University of Edinburgh, the Eidgenössische Technische Hochschule (ETH) Zürich, Fermi National Accelerator Laboratory, the University of Illinois at Urbana-Champaign, the Institut de Ciències de l'Espai (IEEC/CSIC), the Institut de Física d'Altes Energies, Lawrence Berkeley National Laboratory, the Ludwig-Maximilians Universität München and the associated Excellence Cluster Universe, the University of Michigan, the National Optical Astronomy Observatory, the University of Nottingham, The Ohio State University, the OzDES Membership Consortium, the University of Pennsylvania, the University of Portsmouth, SLAC National Accelerator Laboratory,

Stanford University, the University of Sussex, and Texas A&M University.

Based in part on observations at Cerro Tololo Inter-American Observatory, National Optical Astronomy Observatory, which is operated by the Association of Universities for Research in Astronomy (AURA) under a cooperative agreement with the National Science Foundation.

This publication made use of data from Pan-STARRS DR1. The Pan-STARRS1 Surveys (PS1) and the PS1 public science archive have been made possible through contributions by the Institute for Astronomy, the University of Hawaii, the Pan-STARRS Project Office, the Max-Planck Society and its participating institutes, the Max Planck Institute for Astronomy, Heidelberg and the Max Planck Institute for Extraterrestrial Physics, Garching, The Johns Hopkins University, Durham University, the University of Edinburgh, the Queen's University Belfast, the Harvard-Smithsonian Center for Astrophysics, the Las Cumbres Observatory Global Telescope Network Incorporated, the National Central University of Taiwan, the Space Telescope Science Institute, the National Aeronautics and Space Administration under Grant No. NNX08AR22G issued through the Planetary Science Division of the NASA Science Mission Directorate, the National Science Foundation Grant No. AST-1238877, the University of Maryland, Eötvös Loránd University (ELTE), the Los Alamos National Laboratory, and the Gordon and Betty Moore Foundation.

This research made use of NumPy (Van Der Walt et al. 2011), matplotlib, a Python library for publication quality graphics (Hunter 2007), and Astropy, a community-developed core Python package for Astronomy (The Astropy Collaboration et al. 2018).

REFERENCES

- Abbott, T. M. C., Abdalla, F. B., Allam, S., et al. 2018, *ArXiv e-prints*, arXiv:1801.03181
- Abolfathi, B., Aguado, D. S., Aguilar, G., et al. 2018, *ApJS*, 235, 42
- Andrae, R., Fouesneau, M., Creevey, O., et al. 2018, *A&A*, in press, arXiv:1804.09374
- Barber, C., Starkenburg, E., Navarro, J. F., McConnachie, A. W., & Fattahi, A. 2014, *MNRAS*, 437, 959
- Battaglia, G., Helmi, A., Morrison, H., et al. 2005, *MNRAS*, 364, 433
- Bechtol, K., Drlica-Wagner, A., Balbinot, E., et al. 2015, *ApJ*, 807, 50
- Bellazzini, M., Gennari, N., Ferraro, F. R., & Sollima, A. 2004, *MNRAS*, 354, 708
- Belokurov, V., Zucker, D. B., Evans, N. W., et al. 2007, *ApJ*, 654, 897
- Belokurov, V., Walker, M. G., Evans, N. W., et al. 2009, *MNRAS*, 397, 1748
- Besla, G., Kallivayalil, N., Hernquist, L., et al. 2007, *ApJ*, 668, 949
- . 2010, *ApJ*, 721, L97
- Boettcher, E., Willman, B., Fadel, R., et al. 2013, *AJ*, 146, 94
- Bonaca, A., & Hogg, D. W. 2018, submitted to *AAS Journals*, arXiv:1804.06854
- Bovy, J. 2015, *ApJS*, 216, 29
- Boylan-Kolchin, M., Bullock, J. S., & Kaplinghat, M. 2011, *MNRAS*, 415, L40
- . 2012, *MNRAS*, 422, 1203
- Boylan-Kolchin, M., Bullock, J. S., Sohn, S. T., Besla, G., & van der Marel, R. P. 2013, *ApJ*, 768, 140
- Brown, T. M., Tumlinson, J., Geha, M., et al. 2014, *ApJ*, 796, 91
- Casetti-Dinescu, D. I., & Girard, T. M. 2016, *MNRAS*, 461, 271
- Casetti-Dinescu, D. I., Girard, T. M., & Schriever, M. 2018, *MNRAS*, 473, 4064
- Chambers, K. C., Magnier, E. A., Metcalfe, N., et al. 2016, *ArXiv e-prints*, arXiv:1612.05560
- Chiti, A., Frebel, A., Ji, A. P., et al. 2018, *ApJ*, in press, arXiv:1803.01808
- Collins, M. L. M., Tollerud, E. J., Sand, D. J., et al. 2017, *MNRAS*, 467, 573
- Dall'Ora, M., Clementini, G., Kinemuchi, K., et al. 2006, *ApJ*, 653, L109
- Dall'Ora, M., Kinemuchi, K., Ripepi, V., et al. 2012, *ApJ*, 752, 42
- Deason, A. J., Wetzel, A. R., Garrison-Kimmel, S., & Belokurov, V. 2015, *MNRAS*, 453, 3568
- Diaz, J., & Bekki, K. 2011, *MNRAS*, 413, 2015
- Diaz, J. D., & Bekki, K. 2012, *ApJ*, 750, 36
- Diemand, J., Kuhlen, M., & Madau, P. 2007, *ApJ*, 667, 859
- Dinescu, D. I., Girard, T. M., van Altena, W. F., & López, C. E. 2005, *ApJ*, 618, L25
- D'Onghia, E., & Fox, A. J. 2016, *ARA&A*, 54, 363
- Drlica-Wagner, A., Bechtol, K., Rykoff, E. S., et al. 2015, *ApJ*, 813, 109
- Erkal, D., Li, T. S., Koposov, S. E., et al. 2018, submitted to *MNRAS*, arXiv:1804.07762
- Feltzing, S., Eriksson, K., Kleyna, J., & Wilkinson, M. I. 2009, *A&A*, 508, L1
- François, P., Monaco, L., Bonifacio, P., et al. 2016, *A&A*, 588, A7
- Frebel, A., Norris, J. E., Gilmore, G., & Wyse, R. F. G. 2016, *ApJ*, 826, 110
- Frebel, A., Simon, J. D., Geha, M., & Willman, B. 2010, *ApJ*, 708, 560
- Frebel, A., Simon, J. D., & Kirby, E. N. 2014, *ApJ*, 786, 74
- Fritz, T. K., Lokken, M., Kallivayalil, N., et al. 2017, submitted to *ApJ*, arXiv:1711.09097

- Gaia Collaboration, Brown, A. G. A., Vallenari, A., & Prusti, T., e. a. 2018a, *A&A*, in press
- Gaia Collaboration, Helmi, A., van Leeuwen, F., & McMillan, P., e. a. 2018b, *A&A*, in press
- Gaia Collaboration, Lindgren, L., Hernández, J., & Bombrun, A., e. a. 2018c, *A&A*, in press
- Gaia Collaboration, Prusti, T., de Bruijne, J. H. J., et al. 2016, *A&A*, 595, A1
- Garling, C., Willman, B., Sand, D. J., et al. 2018, *ApJ*, 852, 44
- Garofalo, A., Cusano, F., Clementini, G., et al. 2013, *ApJ*, 767, 62
- Garrison-Kimmel, S., Wetzell, A., Bullock, J. S., et al. 2017, *MNRAS*, 471, 1709
- Geha, M., Willman, B., Simon, J. D., et al. 2009, *ApJ*, 692, 1464
- Gill, S. P. D., Knebe, A., Gibson, B. K., & Dopita, M. A. 2004, *MNRAS*, 351, 410
- Gilmore, G., Norris, J. E., Monaco, L., et al. 2013, *ApJ*, 763, 61
- Hansen, T. T., Simon, J. D., Marshall, J. L., et al. 2017, *ApJ*, 838, 44
- Held, E. V., Clementini, G., Rizzi, L., et al. 2001, *ApJ*, 562, L39
- Hunter, J. D. 2007, *Computing In Science & Engineering*, 9, 90
- Ishigaki, M. N., Aoki, W., Arimoto, N., & Okamoto, S. 2014, *A&A*, 562, A146
- Jethwa, P., Erkal, D., & Belokurov, V. 2016, *MNRAS*, 461, 2212
- Ji, A. P., & Frebel, A. 2018, *ApJ*, 856, 138
- Ji, A. P., Frebel, A., Chiti, A., & Simon, J. D. 2016a, *Nature*, 531, 610
- Ji, A. P., Frebel, A., Ezzeddine, R., & Casey, A. R. 2016b, *ApJ*, 832, L3
- Ji, A. P., Frebel, A., Simon, J. D., & Chiti, A. 2016c, *ApJ*, 830, 93
- Ji, A. P., Frebel, A., Simon, J. D., & Geha, M. 2016d, *ApJ*, 817, 41
- Kallivayalil, N., van der Marel, R. P., Alcock, C., et al. 2006, *ApJ*, 638, 772
- Kallivayalil, N., van der Marel, R. P., Besla, G., Anderson, J., & Alcock, C. 2013, *ApJ*, 764, 161
- Kirby, E. N., Boylan-Kolchin, M., Cohen, J. G., et al. 2013a, *ApJ*, 770, 16
- Kirby, E. N., Cohen, J. G., Guhathakurta, P., et al. 2013b, *ApJ*, 779, 102
- Kirby, E. N., Cohen, J. G., Simon, J. D., & Guhathakurta, P. 2015, *ApJ*, 814, L7
- Kirby, E. N., Cohen, J. G., Simon, J. D., et al. 2017, *ApJ*, 838, 83
- Kirby, E. N., Guhathakurta, P., Simon, J. D., et al. 2010, *ApJS*, 191, 352
- Kleyna, J. T., Wilkinson, M. I., Evans, N. W., & Gilmore, G. 2005, *ApJ*, 630, L141
- Klypin, A., Kravtsov, A. V., Valenzuela, O., & Prada, F. 1999, *ApJ*, 522, 82
- Koch, A., & Rich, R. M. 2014, *ApJ*, 794, 89
- Koch, A., Wilkinson, M. I., Kleyna, J. T., et al. 2009, *ApJ*, 690, 453
- Koposov, S. E., Belokurov, V., Torrealba, G., & Evans, N. W. 2015a, *ApJ*, 805, 130
- Koposov, S. E., Gilmore, G., Walker, M. G., et al. 2011, *ApJ*, 736, 146
- Koposov, S. E., Casey, A. R., Belokurov, V., et al. 2015b, *ApJ*, 811, 62
- Koposov, S. E., Walker, M. G., Belokurov, V., et al. 2018, submitted to *MNRAS*, arXiv:1804.06430
- Laevens, B. P. M., Martin, N. F., Ibata, R. A., et al. 2015a, *ApJ*, 802, L18
- Laevens, B. P. M., Martin, N. F., Bernard, E. J., et al. 2015b, *ApJ*, 813, 44
- Lai, D. K., Lee, Y. S., Bolte, M., et al. 2011, *ApJ*, 738, 51
- Lépine, S., Koch, A., Rich, R. M., & Kuijken, K. 2011, *ApJ*, 741, 100
- Li, T. S., Simon, J. D., Pace, A. B., et al. 2018a, submitted to *ApJ*, arXiv:1802.06810
- Li, T. S., Simon, J. D., Kuehn, K., et al. 2018b, submitted to *ApJ*, arXiv:1804.07761
- Libralato, M., Bellini, A., Bedin, L. R., et al. 2018, *ApJ*, 854, 45
- Lux, H., Read, J. I., & Lake, G. 2010, *MNRAS*, 406, 2312
- Marigo, P., Girardi, L., Bressan, A., et al. 2017, *ApJ*, 835, 77
- Martin, N. F., de Jong, J. T. A., & Rix, H.-W. 2008, *ApJ*, 684, 1075
- Martin, N. F., Ibata, R. A., Chapman, S. C., Irwin, M., & Lewis, G. F. 2007, *MNRAS*, 380, 281
- Martin, N. F., & Jin, S. 2010, *ApJ*, 721, 1333
- Martin, N. F., Geha, M., Ibata, R. A., et al. 2016a, *MNRAS*, 458, L59
- Martin, N. F., Ibata, R. A., Collins, M. L. M., et al. 2016b, *ApJ*, 818, 40
- McGaugh, S. S., & Wolf, J. 2010, *ApJ*, 722, 248
- Méndez, R. A., Costa, E., Pedreros, M. H., et al. 2010, *PASP*, 122, 853
- Moore, B., Ghigna, S., Governato, F., et al. 1999, *ApJ*, 524, L19
- Muñoz, R. R., Carlin, J. L., Frinchaboy, P. M., et al. 2006, *ApJ*, 650, L51
- Muñoz, R. R., Geha, M., & Willman, B. 2010, *AJ*, 140, 138
- Musella, I., Ripepi, V., Clementini, G., et al. 2009, *ApJ*, 695, L83
- Nagasawa, D. Q., Marshall, J. L., Li, T. S., et al. 2018, *ApJ*, 852, 99
- Nidever, D. L., Majewski, S. R., & Burton, W. B. 2008, *ApJ*, 679, 432
- Niederste-Ostholt, M., Belokurov, V., Evans, N. W., et al. 2009, *MNRAS*, 398, 1771
- Norris, J. E., Gilmore, G., Wyse, R. F. G., et al. 2008, *ApJ*, 689, L113
- Norris, J. E., Gilmore, G., Wyse, R. F. G., Yong, D., & Frebel, A. 2010a, *ApJ*, 722, L104
- Norris, J. E., Wyse, R. F. G., Gilmore, G., et al. 2010b, *ApJ*, 723, 1632
- Norris, J. E., Yong, D., Gilmore, G., & Wyse, R. F. G. 2010c, *ApJ*, 711, 350
- Okamoto, S., Arimoto, N., Yamada, Y., & Onodera, M. 2008, *A&A*, 487, 103
- . 2012, *ApJ*, 744, 96
- Patel, E., Besla, G., Mandel, K., & Sohn, S. T. 2018, *ApJ*, 857, 78
- Pawlowski, M. S., & Kroupa, P. 2013, *MNRAS*, 435, 2116
- Pawlowski, M. S., McGaugh, S. S., & Jerjen, H. 2015, *MNRAS*, 453, 1047
- Peñarrubia, J., Navarro, J. F., & McConnachie, A. W. 2008, *ApJ*, 673, 226
- Piatek, S., Pryor, C., Bristow, P., et al. 2007, *AJ*, 133, 818
- Piatek, S., Pryor, C., Olszewski, E. W., et al. 2003, *AJ*, 126, 2346
- . 2002, *AJ*, 124, 3198
- Pryor, C., Piatek, S., & Olszewski, E. W. 2015, *AJ*, 149, 42
- Rocha, M., Peter, A. H. G., & Bullock, J. 2012, *MNRAS*, 425, 231
- Roderick, T. A., Jerjen, H., Mackey, A. D., & Da Costa, G. S. 2015, *ApJ*, 804, 134
- Roderick, T. A., Mackey, A. D., Jerjen, H., & Da Costa, G. S. 2016, *MNRAS*, 461, 3702
- Roederer, I. U., & Kirby, E. N. 2014, *MNRAS*, 440, 2665
- Roederer, I. U., Mateo, M., Bailey, III, J. I., et al. 2016, *AJ*, 151, 82
- Sales, L. V., Navarro, J. F., Abadi, M. G., & Steinmetz, M. 2007, *MNRAS*, 379, 1464
- Sales, L. V., Navarro, J. F., Kallivayalil, N., & Frenk, C. S. 2017, *MNRAS*, 465, 1879
- Sand, D. J., Strader, J., Willman, B., et al. 2012, *ApJ*, 756, 79
- Sawala, T., Pihajoki, P., Johansson, P. H., et al. 2017, *MNRAS*, 467, 4383
- Schönrich, R., Binney, J., & Dehnen, W. 2010, *MNRAS*, 403, 1829
- Shipp, N., Drlica-Wagner, A., Balbinot, E., et al. 2018, submitted to *ApJ*, arXiv:1801.03097
- Siegel, M. H. 2006, *ApJ*, 649, L83
- Siegel, M. H., Shetrone, M. D., & Irwin, M. 2008, *AJ*, 135, 2084
- Simon, J. D., & Geha, M. 2007, *ApJ*, 670, 313
- Simon, J. D., Geha, M., Minor, Q. E., et al. 2011, *ApJ*, 733, 46
- Simon, J. D., Drlica-Wagner, A., Li, T. S., et al. 2015, *ApJ*, 808, 95
- Simon, J. D., Li, T. S., Drlica-Wagner, A., et al. 2017, *ApJ*, 838, 11
- Sohn, S. T., Besla, G., van der Marel, R. P., et al. 2013, *ApJ*, 768, 139
- Soszyński, I., Udalski, A., Szymański, M. K., et al. 2016, *Acta Astron.*, 66, 131
- The Astropy Collaboration, Price-Whelan, A. M., Sipőcz, B. M., et al. 2018, *ArXiv e-prints*, arXiv:1801.02634
- Torrealba, G., Belokurov, V., Koposov, S. E., et al. 2018, *MNRAS*, 475, 5085
- van den Bosch, F. C., Lewis, G. F., Lake, G., & Stadel, J. 1999, *ApJ*, 515, 50

- Van Der Walt, S., Colbert, S. C., & Varoquaux, G. 2011, Computing in Science & Engineering, 13, 22
- Venn, K. A., Starkenburg, E., Malo, L., Martin, N., & Laevens, B. P. M. 2017, MNRAS, 466, 3741
- Walker, M. G., Mateo, M., Olszewski, E. W., et al. 2016, ApJ, 819, 53
- Walsh, S. M., Willman, B., Sand, D., et al. 2008, ApJ, 688, 245
- Watkins, L. L., Evans, N. W., & An, J. H. 2010, MNRAS, 406, 264
- Wetzel, A. R. 2011, MNRAS, 412, 49
- Willman, B., Geha, M., Strader, J., et al. 2011, AJ, 142, 128
- Willman, B., Blanton, M. R., West, A. A., et al. 2005, AJ, 129, 2692
- York, D. G., Adelman, J., Anderson, Jr., J. E., et al. 2000, AJ, 120, 1579

APPENDIX

A. TRIANGULUM II

The first spectroscopy of Triangulum II (Tri II) was obtained by Kirby et al. (2015) with Keck/DEIMOS, which was quickly followed up with additional DEIMOS spectroscopy by Martin et al. (2016b). Given the discrepant results between the two studies, Kirby et al. (2017) reobserved the entire sample of member stars identified by Kirby et al. (2015) and Martin et al. (2016b) with DEIMOS. The chemical abundances of the brightest two stars on the red giant branch were studied at high spectral resolution with Gemini-N/GRACES by Venn et al. (2017), and a similar analysis of the brighter star was carried out by Kirby et al. (2017) with Keck/HIRES. Because of its very low luminosity, Tri II contains just two spectroscopically confirmed member stars brighter than $g = 20$, but the three DEIMOS studies produced a total of 32 confirmed non-members brighter than this limit.

B. SEGUE 2

Belokurov et al. (2009) presented MMT/Hectochelle spectroscopy of Segue 2 in the discovery paper for the system, which Kirby et al. (2013a) supplemented with a large Keck/DEIMOS data set. Imaging of Segue 2 by Boettcher et al. (2013) revealed 1 RR Lyrae variable, which was also identified spectroscopically by Kirby et al. (2013a). Roederer & Kirby (2014) analyzed the chemical abundance pattern of the brightest RGB member found by Kirby et al. (2013a) with a high-resolution Magellan/MIKE spectrum. In addition to the dwarf galaxy itself, Belokurov et al. (2009) suggested that a higher metallicity stellar stream with a similar velocity to Segue 2 is present in the same area of the sky. With their smaller survey area, Kirby et al. (2013a) did not find evidence for this additional population. By combining the available data sets, we find a total of 11 spectroscopically confirmed Segue 2 members and 280 confirmed non-members brighter than $g = 20$.³ In addition, 10 stars in the possible foreground stream meet this magnitude cut.

C. HYDRUS I

The most recently discovered Milky Way satellite is Hydrus I (Hyi I), announced just one week ago. In the discovery paper, Koposov et al. (2018) presented Magellan/M2FS spectroscopy of a sample of ~ 30 Hyi I member stars. While nearly all of these stars are bright enough for *Gaia* astrometry, the currently-available preprint only lists the coordinates for 10 stars, the majority of which are non-members and/or are fainter than $g = 20$. Koposov et al. (2018) also identified two RR Lyrae variables in the OGLE-IV Magellanic Cloud RR Lyrae catalog (Soszyński et al. 2016) as Hyi I members. Combining the spectroscopic and RR Lyrae lists, I have 4 confirmed Hyi I members and 5 confirmed non-member stars brighter than $g = 20$.

D. HOROLOGIUM I

Almost immediately after its discovery, Koposov et al. (2015b) published VLT/FLAMES spectroscopy of Horologium I (Hor I). Nagasawa et al. (2018) used VLT/UVES to analyze the chemical abundance patterns of two of the member stars identified by Koposov et al. 2015b as well as a third star selected photometrically (which they confirmed as a Hor I member). Combined, these two samples include 6 spectroscopically-confirmed Hor I members and 13 confirmed non-members brighter than $g = 20$.

E. RETICULUM II

Simon et al. (2015) observed Reticulum II (Ret II) with Magellan/M2FS and Gemini-S/GMOS, which they combined with public VLT/FLAMES spectroscopy from the *Gaia*-ESO survey. The target lists for the three instruments largely overlapped; the VLT data include 6 stars (2 members) not observed by M2FS, and the GMOS data include 1 additional member. Koposov et al. (2015b) independently analyzed the VLT/FLAMES spectra with essentially identical results. A number of authors have studied the chemical abundances of some of the many bright Ret II members with Magellan/MIKE or Magellan/M2FS (Ji et al. 2016a,c; Roederer et al. 2016; Ji & Frebel 2018). In total, there are 22 known member stars and 23 non-members in Ret II at $g < 20$.

³ One star, SDSSJ02192112+2007402, is classified as a non-member by Belokurov et al. (2009) and a blue horizontal branch member by Kirby et al. (2013a). The magnitudes listed for this star by Kirby et al. (2013a) do not match the cataloged magnitudes in

DR7 or any subsequent data release of SDSS, suggesting an error or misidentification. Since the SDSS magnitudes place the star well away from the Segue 2 horizontal branch and the Belokurov et al. (2009) velocity is not consistent with it being a Segue 2 member, I consider it a non-member here.

F. CARINA II

Li et al. (2018a) medium-resolution spectroscopy of Carina II (Car II) with Magellan/IMACS, AAT/AAOmega, and VLT/FLAMES and found 18 member stars. Time-series imaging by Torrealba et al. (2018) identified 5 RR Lyrae variables in the field, of which 3 are at the correct distance to be members of Car II. Two of the Car II RR Lyrae were spectroscopically confirmed as members by Li et al. (2018a), and I assume that the third star is a member as well. Since no public photometry catalogs are available for this part of the sky I use the dereddened magnitudes given by Li et al. (2018a) and remove the reddening correction to obtain apparent magnitudes. The 19 known Car II members are all brighter than $g = 20$, as are a total of 8 confirmed non-members in the field.

G. CARINA III

Carina III (Car III) was observed simultaneously with Car II by Li et al. (2018a), with 4 member stars identified. The stars that are spectroscopically determined to be members of neither Car II nor Car III are mostly located closer to Car II, but in order to provide an astrometric comparison sample of non-members for Car III I consider the same set of 8 stars to be Car III non-members. As with Car II, I remove the reddening correction used by Li et al. (2018a) to determine the observed magnitudes of the Car III stars. Car III has 3 confirmed member stars brighter than $g = 20$.

H. URSA MAJOR II

Martin et al. (2007) and Simon & Geha (2007, hereafter SG07) both observed Ursa Major II (UMa II) with Keck/DEIMOS. Because of the large angular size of the galaxy there is not much overlap between the two studies, and combined they identified a total of 29 member stars. Frebel et al. (2010) followed up the four brightest members on the RGB at high-resolution with Keck/HIRES, finding that one of the four, SDSSJ08500184+6313330, is actually a foreground main sequence star. Time-series imaging by Dall’Ora et al. (2012) uncovered one RR Lyrae variable in UMa II, which is relatively bright (mean V magnitude of 18.39) given the distance of only 35 kpc to UMa II. UMa II has 8 known members and 52 confirmed non-members brighter than $g = 20$.

I. SEGUE 1

Segue 1 was spectroscopically confirmed by Geha et al. (2009), who identified 24 member stars with Keck/DEIMOS. Simon et al. (2011) subsumed the Geha et al. (2009) data set into a much larger DEIMOS spectroscopic survey, finding a total of 71 Segue 1 members. In the interim, Norris et al. (2010b) also obtained AAT spectroscopy of bright stars over a wider field, including one additional Segue 1 member star outside the Simon et al. (2011) coverage area and another member candidate at a radius of $24'$. The entire sample of confirmed Segue 1 red giants has been followed up at high-resolution by Norris et al. (2010a) and Frebel et al. (2014). In total, Segue 1 contains 9 member stars brighter than $g = 20$ (7 RGB stars and 2 HB stars) plus the Norris et al. (2010b) candidate located at a radius of $5.5r_{1/2}$. Thanks to the substantial spectroscopic investment in this field, there are 192 confirmed non-members at $g < 20$ as well.

J. URSA MAJOR I

Ursa Major I (UMa I) has been the subject of three spectroscopic studies. Immediately after its discovery, Kleyna et al. (2005) obtained low S/N, high-resolution spectroscopy of seven stars with the HIRES spectrograph at Keck, five of which they determined were UMa I members. Martin et al. (2007) observed a larger sample of stars at medium resolution with Keck/DEIMOS, including two of the Kleyna et al. members. Finally, SG07 observed UMa I again with DEIMOS and more than doubled the sample of member stars, as well as re-observing all of the stars targeted by Kleyna et al. and most of the members identified by Martin et al.. All of the known bright ($g < 20$) members of UMa I are in the SG07 data set, so I use that sample as my starting point for member selection. In total, there are eight spectroscopically confirmed UMa I members and 33 confirmed non-members at $g < 20$.

K. WILLMAN 1

The first spectroscopy of Willman 1 was obtained by Martin et al. (2007) with Keck/DEIMOS. They classified 14 stars as Willman 1 members, including two red giants brighter than $g = 20$. However, high-resolution spectroscopy of one of the putative bright members with the Hobby-Eberly Telescope by Siegel et al. (2008) showed that it is instead a foreground main sequence star. Siegel et al. confirmed the second RGB star as a member and obtained spectra of 3 non-members at large radii. Willman et al. (2011) observed a much larger sample with Keck/DEIMOS, including both candidates from the Martin et al. (2007) study, and discovered an additional RGB member and two horizontal branch stars. Willman 1 contains four known members and 22 confirmed non-members at $g < 20$.

L. COMA BERENICES

Coma Berenices (Com Ber) has been observed spectroscopically with Keck/DEIMOS by SG07, who found 59 member stars, and Brown et al. (2014), who identified an additional 14 members. Frebel et al. (2010) obtained high-resolution spectroscopy of the brightest three SG07 members. Two RR Lyrae variables in Com Ber were discovered by Musella et al. (2009), both of which are included in the combined spectroscopic sample from SG07 and Brown et al. (2014). There are 12 known stars in Com Ber brighter than $g = 20$ and 29 spectroscopically confirmed non-members brighter than that limit.

M. BOÖTES II

The only multi-object spectroscopic study of Boötes II (Boo II) published so far is that of Koch et al. (2009), who identified a handful of member stars with Gemini/GMOS. Koch & Rich (2014) followed up the brightest Koch et al. member star with Keck/HIRES, and Ji et al. (2016d) obtained high-resolution Magellan/MIKE spectra of three Koch et al. members (including the star analyzed by Koch & Rich 2014) and a fourth bright member identified via yet-unpublished spectroscopy. The chemical abundances of two of these member stars were also studied by François et al. (2016) with VLT/X-Shooter spectra. Despite being one of the least well characterized ultra-faint dwarfs at present, Boo II still contains 4 confirmed member stars and 4 confirmed non-members brighter than $g = 20$.

N. BOÖTES I

Boötes I (Boo I) has been the subject of numerous spectroscopic studies at both medium and high spectral resolution. Radial velocities have been measured by Muñoz et al. (2006, WIYN/Hydra), Martin et al. (2007, Keck/DEIMOS), Norris et al. (2010b, AAT/AAOmega), Kuposov et al. (2011, VLT/FLAMES), and Brown et al. (2014, Keck/DEIMOS). The chemical abundances of Boo I stars have been studied by Feltzing et al. (2009), Norris et al. (2008, 2010b,c), Lai et al. (2011), Gilmore et al. (2013), Ishigaki et al. (2014), and Frebel et al. (2016). Time-series imaging of Boo I has also identified 15 RR Lyrae variables in the galaxy (Siegel 2006; Dall’Ora et al. 2006). As a result of its relatively high luminosity and the extensive follow-up data sets available for Boo I, there are 68 confirmed member stars and 138 confirmed non-members at $g < 20$.

O. DRACO II

Draco II (Dra II) ranks with Boo II as one of the most poorly-studied of the nearby ultra-faint dwarfs. Martin et al. (2016a) obtained Keck/DEIMOS spectroscopy of Dra II, identifying 9 member stars and 25 non-members. Only four of the members are brighter than $g = 20$, with the brightest at $g = 19.4$. No high-resolution chemical abundance studies are available. The online table in Martin et al. (2016a) containing the list of spectroscopic non-members is not currently available, so our sample for the present work includes only the 4 bright members.

P. TUCANA II

Tucana II (Tuc II) was observed spectroscopically with Magellan/M2FS by Walker et al. (2016), who identified 8 member stars. Four of these stars were followed up at higher spectral resolution with Magellan/MIKE to determine their chemical abundances by Ji et al. (2016b). Chiti et al. (2018) observed one additional Walker et al. member, as well as two new member stars selected with SkyMapper photometry, with Magellan/MIKE, so that chemical abundance patterns are now available for the majority of the known Tuc II members. I adopt a membership probability threshold of $p \geq 0.5$ to separate members and non-members in the Walker et al. catalog, but the resulting classifications are not very sensitive to this value (e.g., $p \geq 0.1$ produces identical lists of stars). The union of these data sets results in a total of 10 member stars and 49 confirmed non-members brighter than $g = 20$.

Q. TUCANA III

Simon et al. (2017) obtained medium-resolution Magellan/IMACS spectroscopy of Tucana III (Tuc III), identifying 26 member stars within the core of the satellite. Hansen et al. (2017) studied the chemical abundances of the brightest Tuc III star with a high-resolution Magellan/MIKE spectrum. Ten out of the 26 spectroscopically-confirmed members are brighter than $g = 20$, and Simon et al. (2017) also classified 53 stars at $g < 20$ as spectroscopic non-members.

R. HYDRUS I ASTROMETRIC MEMBER SELECTION

As discussed earlier, the sample of members stars currently available in Hyi I is only 3. However, using the proper motion of Hyi I determined from these 3 stars, a likely complete member sample of Hyi I can be selected from the *Gaia* DR2 catalog. In the left panel of Figure 7 I plot the *Gaia* color-magnitude diagram (CMD) of a field with radius $15'$ centered on Hyi I. The three stars outlined with blue circles are the members identified previously. The red curve is a PARSEC isochrone (Marigo et al. 2017) for a 12 Gyr old population at $[\text{Fe}/\text{H}] = -2.0$, shifted to a distance modulus of 17.20. Because the reddening for faint stars in the *Gaia* bands is not yet well-determined, I assume $A_G = 2 \times E(BP - RP)$ (Andrae et al. 2018) and estimate the extinction empirically by finding the values for which the isochrone matches both the horizontal branch and RGB stars ($A_G = 0.36$ mag, $E(BP - RP) = 0.18$ mag). Choosing the stars with proper motions within 1 mas yr^{-1} of the average value for the Kuposov et al. (2018) members produces a clear set of red giant branch stars in the CMD. As a final step, I select the stars that are both within 0.08 mag of the RGB (0.30 mag on the HB) and have proper motions within 2σ of the Hyi I value in Table 3. I find 41 such stars brighter than $G = 20$ in the DR2 catalog, which trace out a well-defined RGB and horizontal branch in the CMD, and are tightly clustered in proper motion space (Fig. 7). In this way, starting from just 3 member stars one can identify a highly pure sample of member stars that will greatly improve the efficiency of future spectroscopic observations. Of course, Hyi I is a particularly easy case given its relatively high luminosity and modest distance, but similar methods can certainly be applied to other dwarfs. With this 41 star sample the proper motion uncertainties for Hyi I are reduced by a factor of ~ 5 to $\sim 0.03 \text{ mas yr}^{-1}$ in each coordinate, close to the DR2 systematic floor. However, the orbit is essentially unchanged.

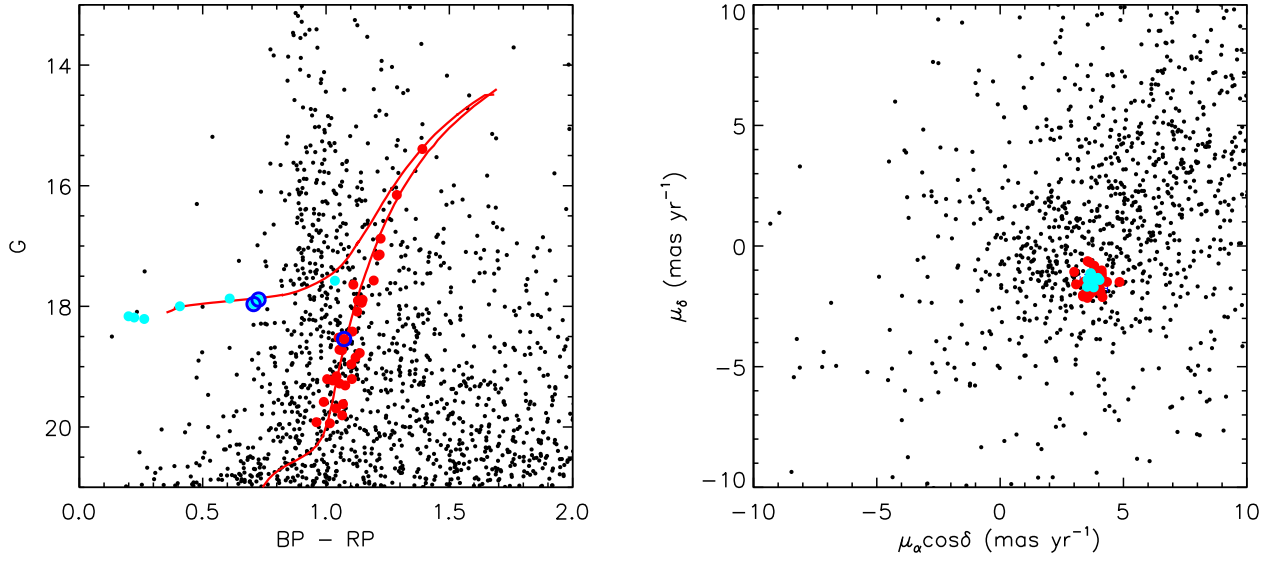


FIG. 7.— (left) *Gaia* color-magnitude diagram of Hyi I. The 3 known member stars are outlined in blue, and the proper motion + color-selected candidates are displayed as filled red (cyan) circles on the RGB (HB). The red curve is a PARSEC isochrone an age of 12 Gyr and a metallicity of $[\text{Fe}/\text{H}] = -2.0$. (right) Proper motion diagram of the same stars.